Introduction and Literature Review

1.1 Introduction

Interstitial-free (IF) steels find applications in the automotive industries for the fabrication of complicated body parts due to their high formability and high planar anisotropy. However, the lower strength of the material demands higher section thickness leading to an increased mass and consequent decreased fuel efficiency [Hoile 2000, Purcek et al. 2012]. It has been suggested that the strength can be improved significantly by the grain refinement [Song et al. 2006]. The grain size can be reduced to an ultrafine level by severe plastic deformation (SPD) techniques [Valiev et al. 2006], among which Equal- Channel Angular Pressing (ECAP) has become a popular technique because it can be applied for producing reasonably homogeneous microstructure in fairly large billets of wide range of alloys to intermetallics, metal-matrix composites to synthesize fully dense, bulk ultrafine-grained (UFG) materials [Purcek et al. 2012, Song et al. 2006, Valiev et al. 2006, Iwahashi et al. 1998, Gazder et al. 2011, Hadzima et al. 2007, Valiev et al. 2002]. In general, the microstructural refinement is dependent on the amount of strain, type of routes as well as the geometry of the die [Valiev et al. 2006, Manna et al. 2008, Manna et al. 2012]. The degree of refinement in IF steel increases with increasing amount of equivalent strain per pass, increasing of the severity or decreasing the intersection angles [Li et al. 2007] and amount of total equivalent strain [Gazder et al. 2008, Li et al. 2006, Hazra et al. 2011]. Among these, the amount of strain has a strong effect on the microstructural modification. Major

factors that are responsible for the improved mechanical behavior are understood to be grain size, grain boundary nature and distribution and the evolution of dislocations. Along with microstructure, texture evolution also depends on amount of deformation, channel intersection angles and rotation of sample after each pass. Depending upon crystallographic structure and slip systems of material, specific texture components are generated by crystal reorientation in macroscopic shear plane and direction [Higuera et al. 2013, Li et al. 2007]. ECAP can be applied to the IF steel for successful production of bulk and sheet materials with excellent mechanical properties, such as high strength. However, the ultrafine-grained (UFG) microstructure brings about limited ductility with a few percent uniform elongation because of the reduced dislocation motion and accumulation ability [Ma, Wang et al. 2004]. Considering the application, a reasonable combination of high strength and good ductility for IF steel is mandatory. The ductility of UFG materials can be enhanced without considerable loss of strength by appropriate annealing treatments after severe plastic deformation (SPD). This improvement was attributed to the bimodal grain size distribution introduced into the deformed microstructure of Cu with micrometer sized grains embedded inside a matrix of nanocrystalline and ultrafine (<300 nm) grains [Wang et al. 2002]. For that purpose the annealing process can be applied to UFG materials processed by SPD techniques to obtain a microstructure with increased stability. There is abundance of literature dealing with changes in microstructure, texture and mechanical properties at low strain level whereas no literature to show these effects at large strain level.

1.2 Interstitial-Free Steel

Interstitial-Free (IF) steels is very soft steel due to the reason that there are no interstitial solute atoms to strain the solid iron lattice. IF steel have non-ageing character and no yield point elongation. IF steel containing only Ti is used to produce the best mechanical properties for deep drawing applications [Wang 2006]. IF steel is also stabilized with both Ti and Nb. To get carbon content in range between 0.01 and 0.04 weight percent material is processed through a bottom blown (Q-BOP) or top blown (BOP) process [Miller et al. 1998, Turkdogan et al. 1998, Nilles et al. 1979]. Dissolved gases (such as hydrogen and nitrogen, and carbon/oxygen) in liquid steel are removed using vacuum in the form of CO and CO_2. Now liquid melt is processed through vacuum degasser to get ultra-low level of carbon (C<0.005 weight percent) [Kor et al. 1998, Takahashi et al. 1995, Kishimoto et al 1993, Stouvenot et al. 1998]. There are advanced technologies for this purpose as Vacuum Tank Degassing (VTD), Vacuum Arc Degassing (VAD), Vacuum Oxygen Decarburization (VOD) Vacuum Degassing–Oxygen Blowing (VD-OB) and circulation processes such as the Dortmund-Horder (DH) and Ruhrstahl Heraeus (RH) processes. After degassing process, Al is added to deoxidize the steel. Removal of nitrogen content to ultra-low level (<40 ppm) is necessary. The gases (such as CO) present in the process of oxygen steelmaking provide stirring action to reduce nitrogen levels. Finally removal of sulphur from steel is done by inoculation of reagents such as magnesium, lime, and calcium carbide in liquid steel to stabilize interstitial. Desulfurization can reduce sulphur levels to <0.004 weight percent. Remaining sulphur can be removed during vacuum degassing by introducing the reagent after deoxidation of the steel. After control of carbon, nitrogen and sulphur during steel making and casting Ti and Nb are added in ladle to stabilize carbon in the form of precipitates [Osman et al. 2001]. For

the production of deep-drawing steel strip the slab is reheated and subsequently rough rolled and finish rolled to its final hot strip thickness in the austenite temperature region. This hot strip is cooled to low temperature and coiled.

Conventional IF steels have ferrite grains (15-250 μm) [Saray et al. 2011, Purcek et al. 2012, Janecek et al. 2014, Kuroda et al. 2006, Hadzima et al. 2007] that provide can have ultimate tensile strength between 200-400 MPa, yield strength 150-250 MPa and elongation (30-60)% [Osman et al. 2001, Toroghinejad et al. 2006, Saray et al. 2012]. Toroghinejad et al. [Toroghinejad et al. 2006] have reported yield strength of 278±3 MPa and 40% total elongation in hot rolled IF steel slab of 0.012 wt.% carbon. Formability exceeds >1.8 for IF steel whereas, rarely exceeds 1.8 for traditional Al killed steel [Hoile 2000]. Interstitial content in IF steel is <0.003 wt % C and <0.004 wt % N [Banerjee 2012]. IF steel are non-aging because carbon is combined as precipitates rather than solid solution. The extra deep drawn steels are used for automotive applications like rear floor pan, the spare wheel well and front and rear door inners [Hoile 2000]. Interstitial atoms, such as carbon and nitrogen, have a marked effect on the deformation behaviour of steel. Discontinuous yielding in low carbon steel is strongly related to interstitial species. Solute carbon and nitrogen may also degrade the formability (in particular work hardening) of steel. Furthermore, discontinuous yielding is related to Lüders bands formation, which is unfavourable to surface appearance and may also result in premature breakage during forming [Osman et al. 2001]. Addition of Titanium and Niobium is typically to stabilize interstitial species [Banerjee 2012, Bayraktar et al. 2009]. The solutes are removed by precipitation of AlN, TiN, TiS, TiC, and Nb (C,N) at grain boundaries, subgrain boundaries and free surfaces [Hook et al. 1975, Sato et al. 1994, Hua et al. 1995, Hua et al. 1993, Tither et al. 1994, Ardo et al. 1995].

It has been suggested that the strength of IF steel can be improved significantly by the grain refinement. The grain size can be reduced to an ultrafine level (100 nm to <1 µm) by severe plastic deformation (SPD) techniques, such as high pressure torsion, accumulative roll bonding, multi directional forging, twist extrusion and equal channel angular pressing (ECAP). Among the SPD techniques, ECAP is a popular technique due to simple shear deformation as sample undergoes no change in dimensions of work piece, ability to impart large strains by repetitive operations, homogeneity in deformation, control over microstructure and texture to some extent, and larger billet dimensions compared to the other SPD methods [Saray et al. 2011, Semiatin et al. 2000]. The degree of refinement in IF steel increases with increasing amount of total equivalent strain, amount of equivalent strain per pass and increase of the severity or decrease the intersection angles.

These steels are selected for body parts of complicated shapes due to high formability but they lack in strength. Grain refinement can enhance strength of materials and can be described by Hall Petch relationship [Valiev et al. 2006]. There are different types of grain boundaries (low angle, high angle, equilibrium and non-equilibrium) formed, depending on regime of SPD [Valiev et al. 2000, Valiev et al. 2008]. These regimes pave the way to grain boundary engineering or to control the properties of materials by varying the grain boundary structure.

1.3 SPD Techniques

Severe plastic deformation (SPD) processes are plastic deformation techniques by which a large amount of strain is imposed on the material without altering much the dimensions or cross section [Valiev et al. 2006]. As the dimension of the workpiece is not altered, it can be deformed repeatedly. The imposed strain is utilised to change the microstructure/texture that in turn modifies the properties of the

materials. SPD processes impose very high plastic strain in a metal in order to cause the grain refinement so that coarse grained material is broken down into finer grain sizes. Some of these processes are Equal-channel angular extrusion or pressing (ECAE/P), high pressure torsion (HPT), accumulative roll bonding (ARB) and multi-axial compression/forging (MAC/F). Among the processing method discussed, some like ECAE/P, MAC/F and HPT introduce severe plastic deformation on bulk materials, while others like ARB on sheet materials.

1.3.1 High Pressure Torsion (HPT)

High pressure torsion (HPT) is a severe plastic deformation technique by which small discs typically of 10 mm diameter and 0.2 mm thickness are deformed by torsion in a constrained disc (Figure 1.1) by applying high pressure (usually 1-10 GPa) [Kawasaki et al. 2014]. Only small coin-shaped samples, usually 10–20 mm diameter and 0.1-2 mm thickness [Klöden et al. 2009, Zhilyaev et al. 2008, Zhilyaev et al. 2001, Song, Wang et al. 2012, Song Wang et al. 2013, Janecek et al. 2014, Sakai et al. 2005] can be processed. The sample is in the form of a disk, located between anvils where compressive pressure is applied and it is subjected to torsional strain, imposed through lower anvil (Figure 1.1). The sample is deformed through surface frictional forces. Shear strain at a distance r from centre can be given by [Zhilyaev et al. 2003, Valiev, Ivanisenko et al. 1996, Wetscher et al. 2004]

$$\gamma = \frac{2\pi N r}{h} \tag{1.1}$$

And equivalent shear strain (or von Mises' equivalent strain) can be

$$\varepsilon_{eq} = \frac{\gamma}{\sqrt{3}} \tag{1.2}$$

Where N is the number of revolutions, h is the disk thickness, r is the radius of the disk. Distribution of shear strain is nonuniform in this process as at rotation axis it is zero and increases linearly in radial direction. In this process severity of strain can

be achieved by number of revolutions of anvil [Zhilyaev et al. 2001, Zhilyaev et al. 2005, Horita et al. 2005] through friction between the disc-shaped sample and a rotating plunger but that results in almost uniform distribution of UFGs. Estrin et al. have reported on the basis of microstructural modelling that uniform strain and homogeneous microstructure can be achieved by this process [Estrin et al. 2008, Estrin et al. 2013]. HPT is utilised for grain refinement from 0.5 mm to ~200 nm in Al–Mg–Sc alloy [Sakai et al. 2005]. There is significant variation in the values of the microhardness and microstructure along the diameters of disks processed by HPT for IF steel with lower hardness values in the centre and higher values in the peripheral regions of the disks [Song et al. 2012, Song et al. 2013, Janeček et al. 2014]. Janeček et al. have reported inhomogeneous microstructure with 400-500 nm grains at centre, 250-300 nm grains at half radius and 200-250 nm grains at the edge of disc shaped samples deformed upto 5 revolutions. Hardness also varied correspondingly from 214 HV at centre to 355 HV at the edge [Janeček et al. 2014]. Grain size reduces to 308 nm by recrystallization process at 1 revolution of HPT process by applying 2.5 GPa pressure in IF steel. Formation of low angle grain boundaries is found within large grains with increased fraction of high angle grain boundaries which results in increase in hardness of >350 HV [Song et al. 2013].
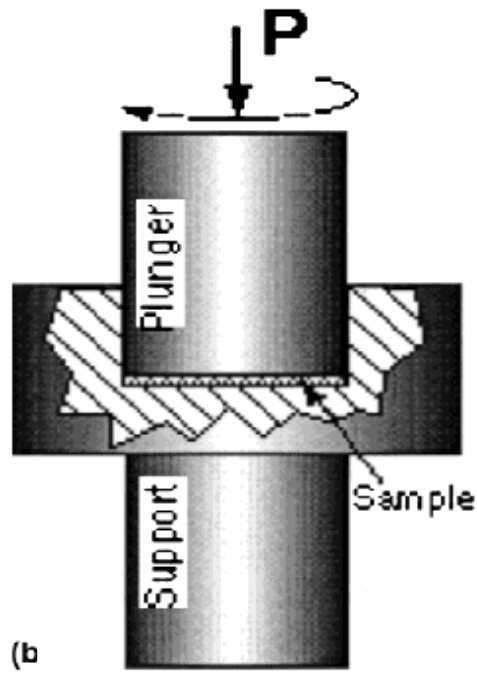
Figure 1.1: Schematic diagram of HPT [Valiev et al. 2002]

1.3.2 Accumulative Roll-Bonding (ARB)

Accumulative roll-bonding (ARB) was introduced by Saito et al. [Y. Saito et al. 1999] as the low productivity of the ECAP and the small work-piece size of HPT impose limitations. In this technique a metal sheet is rolled to 50% thickness reduction and cut in two halves then stacked together, thus original thickness of sheet is restored. Before stacking the two joining surfaces are de-greased, wire brushed stacked and then rolled together (Figure 1.2). This process is repeated till required total amount of strain is imposed. The surfaces of sheet are cleaned and brushed each time to avoid difficulty in bonding. Total equivalent shear strain can be given by [Geist et al. 2011]

$$\varepsilon_{eq} = \frac{2N}{\sqrt{3}} \ln\left(\frac{l_0}{l}\right) \tag{1.3}$$

Where l_0 is thickness of sample, l is thickness of sample after rolling and N is number of passes. There is abundance of literature on application of ARB on commercial pure Al, Al-Mg alloy and interstitial-free steel [Hausol et al. 2010]. ARB

8

is used to make Al metal matrix composite by sheath rolling method [Lee et al. 1999]. IF steel processed by ARB process for grain refinement from 0.3 to 10 μm leads to increase in strength from 303 MPa to 819 MPa [Tsuji et al. 2002]. Jamaati et al. [Jamaati et al. 2015] have reported that the grain size of IF steel is decreased to smaller than 100 nm range after equivalent strain of 6.4. They have reported increase in yield strength to 909 MPa from 84 MPa of initial sample [Jamaati et al. 2015]. Lee et al. [Lee et al. 2004] have deformed IF steel upto equivalent strain of 7.1 and strength got increased from 0.28 GPa to 1.12GPa. Yoda et al. 2011 [Yoda et al. 2011] have reported decrease in Erichsen value with grain size after equivalent strain 0.3 of ARB process. When as-received IF steel was deformed by ARB for equivalent strain 8, microstructure get refined to UFG (>500 nm) size and hardness increased from 98 HV to 247 HV [Tamimi et al. 2014]. They also have reported higher hardness (>210HV) value at lower preheating temperature 450°C of ARB process however, undesired unbounded area is found. The evolution of microstructure of IF steel is monitored during ARB upto equivalent strain of 8 by Reis et al. The microstructural development shows that lamellar features are forming at medium strains of < 5.6 which gradually transforms into more equiaxed structures at the very high strains of >= 6.3. The average lamellar width continue to decrease and at the 6th pass (ε_{vM} >= 4.8) the fraction of HAGB increases while the grain size remains constant [Reis et al. 2005].
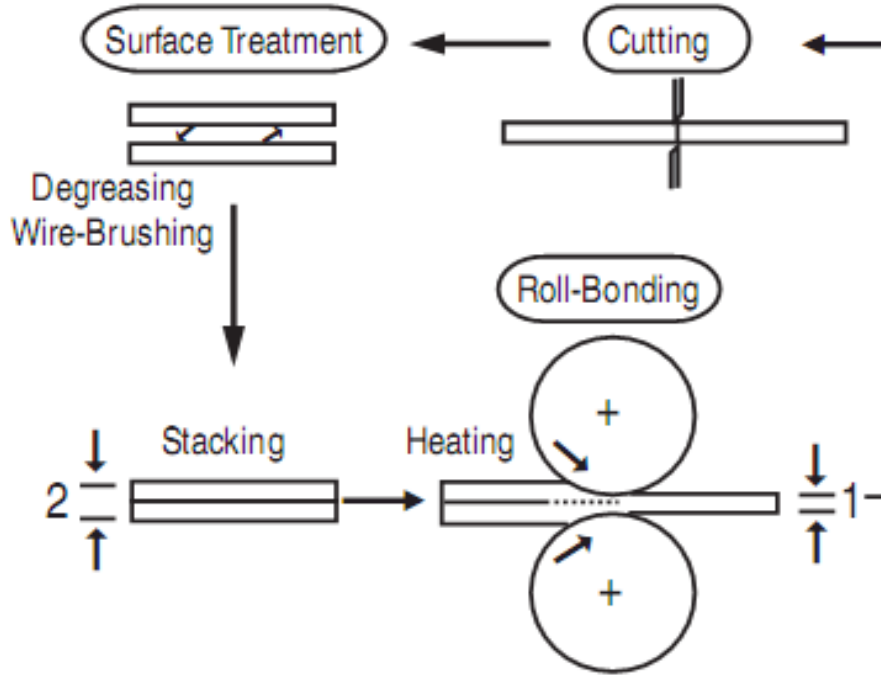
Figure 1.2: Schematic diagram of ARB process [Y. Saito et al. 1999]

1.3.3 Multi-Directional Forging (MDF)

Multi-directional forging (MDF) is a SPD technique introduced in 1990s [Galeyev et al. 1990, Salishchev et al. 1995]. MDF operates in three orthogonal directions by repeated settings. In forging, during every pass forging axis is changed by 90°. In this process sample size and aspect ratios are constant so that unlimited equivalent strain (ε_{vm}) can be applied till sample get fractured [Estrin et al. 2013].

$$\varepsilon_{eq} = N \frac{2}{\sqrt{3}} \ln(\frac{a}{b}) \qquad (1.4)$$

Where N is number of cycles, a and b are sample dimensions. Grain refinement mechanism operative during MDF is a dynamic recrystallization process at $0.1\text{-}0.5T_m$. Microstructure produced by MDF is less homogeneous than ECAP or HPT [Estrin et al. 2013]. Using this technique, Ti–6Al–4V alloy has been deformed to cumulative strain of 3 and UFGs of 0.3μm are produced with tensile strength of 1360 MPa and 7% elongation [Zherebtsov et al. 2004]. Soleymani et al. have deformed low carbon steel by MDF upto an equivalent strain of 2.8 and reported increase in yield

strength from 345 to 850 MPa, ultimate tensile strength from 457 to 1115 MPa, and decrease in elongation from 25.8 to 7.1% after ferrite grain refinement from 38µm to 1.2 µm [Soleymani et al. 2012].

1.3.4 Twist Extrusion (TE)

Twist extrusion (TE) is alternative of simple shear deformation process, introduced by Beygelzimer [Beygelzimer et al. 1999, Y. Y. Beygelzimer et al. 2002]. In this process, a sample is extruded using a special extrusion die. This process is combination of torsion with extrusion (Figure 1.3).
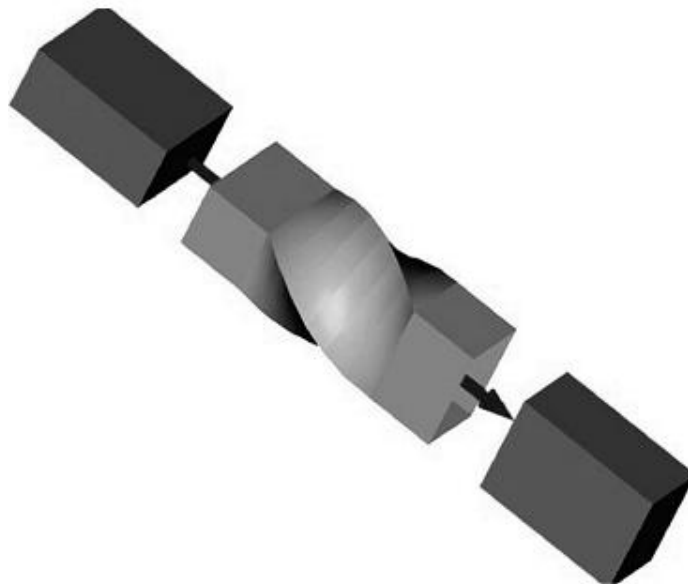
Figure 1.3: Schematic diagram of twist extrusion die and work piece [Beygelzimer et al.2006]

Sample can be extruded many times to accumulate large strain by maintaining original dimensions of work piece. Equivalent strain can be calculated by [Estrin et al. 2013]

$$\varepsilon_{eq} = N \frac{2}{\sqrt{3}} tan\gamma \qquad (1.5)$$

Where γ is the twist line slope and N is number of passes. The advantage of this process is its high up scaling capacity whereas; drawback of this process is non-uniform deformation (smallest near the extrusion axis) [Estrin et al. 2013]. Orlov et al.

have shown that this technique is less effective in producing UFG structure than ECAP or HPT [Orlov et al. 2009]. Pashinska et al. [Pashinska et al. 2012] have reported 84% high angle grain boundaries after deforming low carbon steel upto equivalent strain 6 and grain size refined from 15μm to 5 μm. At equivalent strain of 4.8, strength is reported to be 213 MPa and elongation to be 38% [Orlov et al. 2009].

1.3.5 Equal-channel Angular Pressing (ECAP)

Equal-channel angular pressing (ECAP) is a SPD technique in which billet is deformed through two intersecting channels of equal cross section by simple shear without changing cross section of billet. The principal of ECAP process is illustrated in schematically in Figure 1.4. A sample is pressed through an ECAP die using a plunger. Plunger is normally pressed by a press ram.
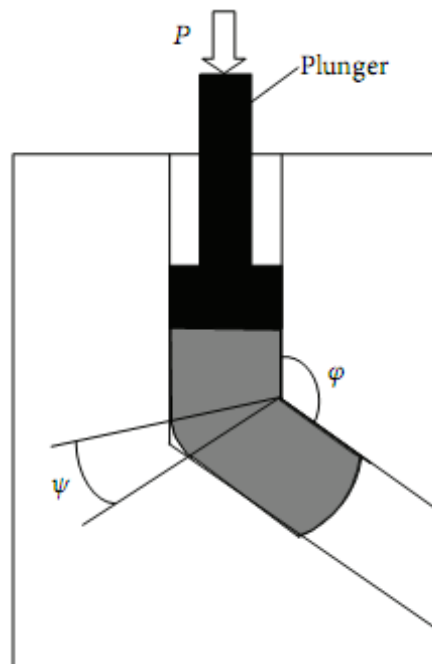
Figure 1.4: Schematic diagram of the die channel [Azushima et. al 2008].

A simple shear deformation is imposed as the sample passes through the die as shown in Figure 1.5. The theoretical shear plane is shown between two adjacent element within the sample numbered as 1 and 2. The elements are transposed as

depicted in Figure. The sample ultimately emerges from the die without any change in cross-sectional dimensions. However, the end surface of the sample is closely parallel to the shear plane. The ECAP die consists of two channels of equal cross section intersecting at an inner intersection angle Φ and outer arc angle ψ. At every passage shear strain is imposed on the billet. The imposed strain is responsible for microstructural modifications. The parameters like strain per pass, total imposed strain, rate of deformation, temperature, process routes, friction between die and billet and back pressure, shearing patterns and slip system of material influence microstructural modifications [Valiev et al. 2006]. ECAP process was first introduced by Segal and his co-workers in the 1970s and 1980s at an institute in Minsk in the former Soviet Union [Segal et al. 1981, Segal patent 1977] to introduce high strain to the metal by simple shear deformation. Later on in 1990s ECAP became popular to produce metals with ultrafine and submicron grains with greatly enhanced properties [Segal 1977, Valiev et al. 1991, Valiev et al. 1993, Valiev 1996].
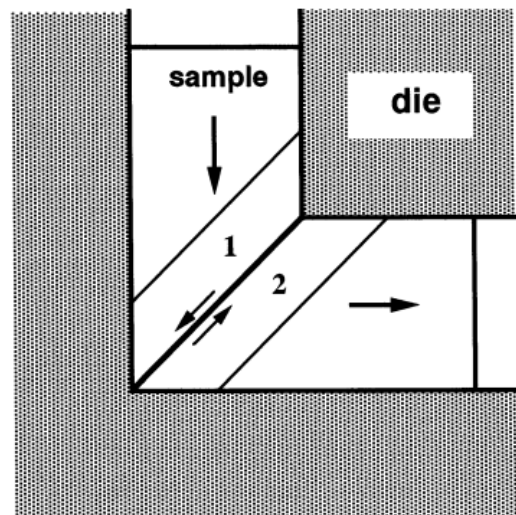
Figure 1.5: The principle of ECAP showing the shearing plane within the die
[Nakashima et al. 2000].

a. **Influence of Imposed Strain**

The imposed shear strain ($\gamma1$) per pass strongly depends on inner intersection angle Φ and outer arc angle ψ and for route A can be calculated by the following equation [Iwahashi et al. 1996]

$$\gamma_1 = \left[2\cot\left(\frac{\Phi}{2} + \frac{\Psi}{2}\right) + \psi\cosec\left(\frac{\Phi}{2} + \frac{\Psi}{2}\right) \right] \tag{1.6}$$

Where Φ and ψ are in radian. This shear strain is accumulative and total shear (γ) for N number of passes can be given by

$$\gamma = N\left[2\cot\left(\frac{\Phi}{2} + \frac{\Psi}{2}\right) + \psi\cosec\left(\frac{\Phi}{2} + \frac{\Psi}{2}\right) \right] \tag{1.7}$$

By equivalence of spent energy, von Mises' equivalent strain (ε_{vm}) is calculated from shear strain (γ) for N number of passes by the following equation [Iwahashi et al. 1996]

$$\varepsilon_{vm} = \frac{N}{\sqrt{3}}\left[2\cot\left(\frac{\Phi}{2} + \frac{\Psi}{2}\right) + \psi\cosec\left(\frac{\Phi}{2} + \frac{\Psi}{2}\right) \right] \tag{1.8}$$

Figure 1.6 is graphical representation of Eq. (1.7) and demonstrates correlation of an inner intersection angle Φ (from angular range 45 to 180°) on an outer arc angle of Ψ (from angular range 0 to 90°) with equivalent strain (for single pass). Based on Figure 1.6 it can be concluded that high strain can be accumulated when die angles Φ and Ψ are small. The magnitude of strain imposed has major influence from angle Φ but minor effect from outer arc angle Ψ [Furuno et al. 2004].
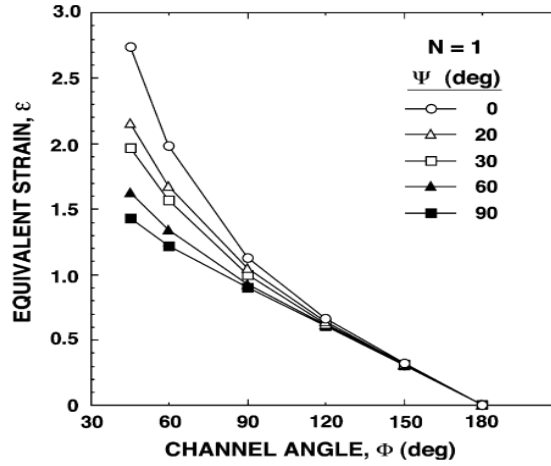
Figure 1.6: Variation of the equivalent strain with the channel angle Φ over angle Ψ [Furuno et al. 2004]

The properties of the materials are strongly dependent on the plastic deformation behaviour during pressing, which is governed mainly by die geometry (a channel angle Ø, corner angle Ψ), material properties (strength and hardening behaviour) and process variables (temperature, lubrication and deformation speed). The deformation during ECAP occurs within the localized zone in the fan-shaped area [Semiatin et al. 2000]. There is large shear plastic deformation in the fan shaped area or main deforming zone when the die corner angle Ψ is 0°, deformation occurs in the immediate vicinity of the plane, i.e. the shear plane. Inhomogeniety increases with higher die angle, round die corner, lower length to diameter ratio and number of passes [Djavanroodi et al. 2012, Basavaraj et al. 2009, Wei et al. 2006, Kim et al. 2004]. Segal [Segal 1997, Segal 1999] has derived equivalent ratios for other deformation techniques based on equivalence of spent energy adopting route A from the shear strain (γ) imposed by ECAP process. These ratios are equivalent extrusion reduction ratio, equivalent rolling reduction ratio. The equivalent or effective extrusion reduction ratio ($\lambda_E = F_0/f$) can be calculated from the following equation

$$\lambda_E = e^{\frac{N\gamma_1}{\sqrt{3}}} \tag{1.9}$$

Equivalent or effective rolling reduction ratio ($\lambda_R = A_0/A$) can be found out from the following equation

$$\lambda_R = e^{\frac{N\gamma_1}{2}} \tag{1.10}$$

Where extrusion area reduces from f_0 to f and area of rolled sheet decreases from A_0 to A. N is number of passes and γ_1 is shear strain per pass.

Equivalent distortion of microstructural elements like equivalent or effective elongation ratio (λ_l), equivalent or effective aspect ratio (λ_m) and equivalent or effective thinning ratio (λ_a) can be calculated from the following equation

$$\lambda_l = (1 + N^2\gamma_1{}^2)^{\frac{1}{2}} \tag{1.11}$$

Equivalent or effective aspect ratio

$$\lambda_m = (1 + N^2\gamma_1{}^2)^{\frac{2}{3}} \tag{1.12}$$

Equivalent or effective thinning ratio

$$\lambda_a = 1 + N^2\gamma_1{}^2 \tag{1.13}$$

b. **Effect of Routes on ECAP Process**

For regular polygon shaped sample such as square, hexagon or circle if sample is rotated between consecutive passes shearing will be caused in different planes. Figure 1.7 represents different routes for ECAP process. In route A, the sample is not rotated with respect to its axis between two consecutive passes, in route B_A sample is rotated 90° in alternate directions and in route B_C sample is rotated 90° either clock wise or anti-clockwise between passes always in one direction only and in route C sample is rotated 180° between passes about its axis. Results show that in route B_C material is deformed on all X, Y and Z planes after 4 passes [Furukawa et al. 1998]. Hazra et al. [Hazra et al. 2011] have reported 63% high angle grain boundaries in the

microstructure of IF steel at ε_{vm}=9.2 following route Bc in ECAP process. In route E, sample follows 2C X 2C where after 2C sample is rotated 90° between 2 sets of rounds [Barber et al. 2004]. In route E material gets uniformly strained compared to other routes.
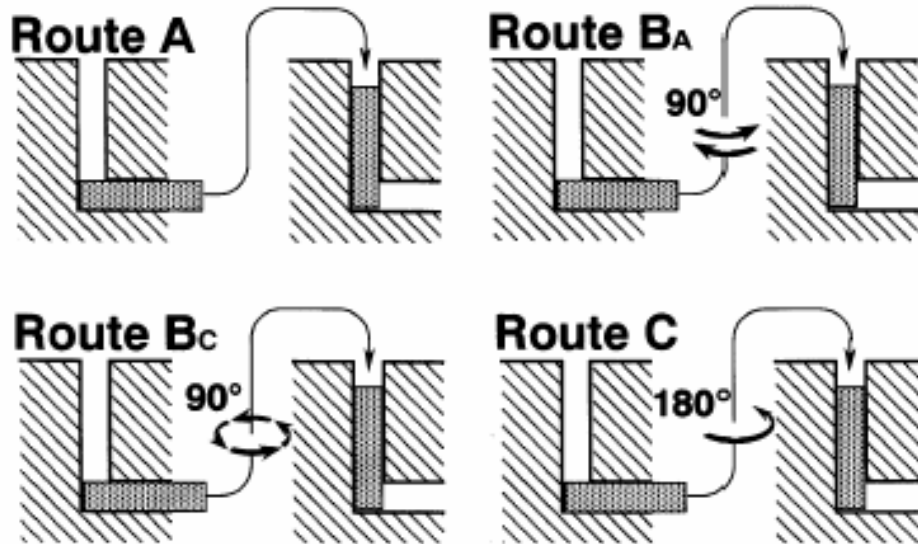
Figure 1.7: Routes for ECAP processing [Estrin et al.2005].

In route A, unidirectional straining (route A), continuous evolution of the texture results in build up of misorientations between cell blocks [Prangnell et al. 2004]. When material is deformed using route Bc of ECAP process, orthogonal changes in strain path can cause instability and shear banding due to reduction in the glide stress for the movement of subsequent dislocations. Moreover, activation of a new set of slip systems result in increased yield stress because the already formed DDWs act as barriers to slip [Rauch 1992, Rauch et al. 1989, Prangnell et al. 2004]. In route Bc, isotropic submicron grain structures are formed along with localization of shear dominated with equiaxed submicron grains and undeformed regions [Prangnell et al. 2004]. Rate of microstructural refinement is found to be more in case of route Bc than other routes during ECAP of IF steel [Gazder et al. 2008]. During deformation and direct reversal of strain path, density of dislocation walls get reduced

as dislocations of opposite sign are injected on same slip system [Hasegawa et al. 1975].

The nose and tail regions of billet get affected strongly by the routes. The end effect is maximum for the route A, intermediate for the route BC and minimum for the route C [Agnew et al. 2005]. The commercial AA7050 aluminium alloy in the solution heat-treated condition was processed by ECAP through routes A and B_C at 150°C upto 6 passes. After one pass ($\varepsilon_{vm}=0.6$), subgrains are formed of thicker walls and are better defined after more number of passes. The samples processed for three ($\varepsilon_{vm}=1.8$) and six passes by route A contains elongated subgrains. Subgrains of 200 nm width are after formed after three passes while after 6 passes ($\varepsilon_{vm}=3.6$), width of the subgrains get slightly reduced to 100-200 nm. Whereas, microstructure of samples processed by route B_C is formed by smaller equiaxial subgrains or cells than those obtained from route A. Moreover, high density of dislocations is located at cell boundaries which are independent of the route. Hardness variation shows that ECAP of commercial AA7050 aluminium alloy at 150°C results in increase of hardness even after the first pass due to precipitation, microstructure refinement and also from work hardening. When the number of passes increases to three ($\varepsilon_{vm}=1.8$), a further strengthening is observed and remains constant up to six passes ($\varepsilon_{vm}=3.6$) by route B_C. After six passes of ECAP by route A, the hardness value is similar to as that of one pass sample ($\varepsilon_{vm}=0.6$) [Cardoso et al. 2011].

c. **Effect of Pressing Speed, Friction and Back Pressure**

Pressing speed has a significant effect on microstructure of material to be deformed. When pressing speed is slow, microstructural changes takes place at a slow rate but at high speed deformation take place abruptly and temperature of sample increases leading to recovery/recrystallization of microstructure. Back pressure

exerted by using an additional ram in exit side increases workability and uniformity in metal forming and resists cracking thereby sample damage can be hindered [Hashmi 2014, Lapovok 2005]. Oh et al. [Oh et al. 2003] have reported larger effective strain values per passage by using the back pressing plunger. However, Djavanroodi et al. [Djavanroodi 2010] have reported that there is no noticeable effect on the magnitude of the strain imposed on the sample but there is a decrease in dead zone. Inhomogeneity parameter decreases when the back pressure value increases from 50 MPa to 400 MPa. [Nejadseyfi et al.2015]. Shear zone also increases and uniform material flow is obtained with back pressure [de Barros et al. 2013]. Usually, the deformation of billet is uniform at the centre only. The front end or nose and back end or tail, are less deformed. The nose and tail regions of the billet will increase with without back pressure [Oruganti et al. 2005, Bowen et al. 2000] and number of passes [Rusin et al. 2006, Zhang et al. 2007, Beyerlein et al. 2009]. Friction between material and die acts as back pressure and helps in filling gaps between sample and die outer corner, top and bottom surfaces of the exit channel but higher friction increases heterogeneity [Li et al. 2004, Oruganti et al. 2005, Bowen et al. 2000]. The central uniform region shrinks with number of passes [Beyerlein et al. 2009]. Friction between channel and work piece may result in metal sticking to the tools by the application of high pressure and rough billet surface [Segal 1999]. Friction is minimized by finishing the sample, polishing metallographically and applying lubricants like graphite or molybdenum-di-sulphide to the sample and die meeting surface. The effect of ram speed and friction is very less as compared to the back pressure effect [Nejadseyfi et al. 2015]. As strengthening of material is strongly dependent on temperature, load required to deform the material by ECAP increases with decreasing temperature [Venkatraman et al. 2013]. There is limitation with

conventional ECAP processing that the sample has to be reinserted repeatedly to impose large amount of strain. To save the time and labour other methods are evolved like rotary-die ECAP, side extrusion, parallel channels and multi pass ECAP. In ECAP process of IF steel friction leads to more accumulated strains and strain heterogeneity [Medeiros et al. 2008].
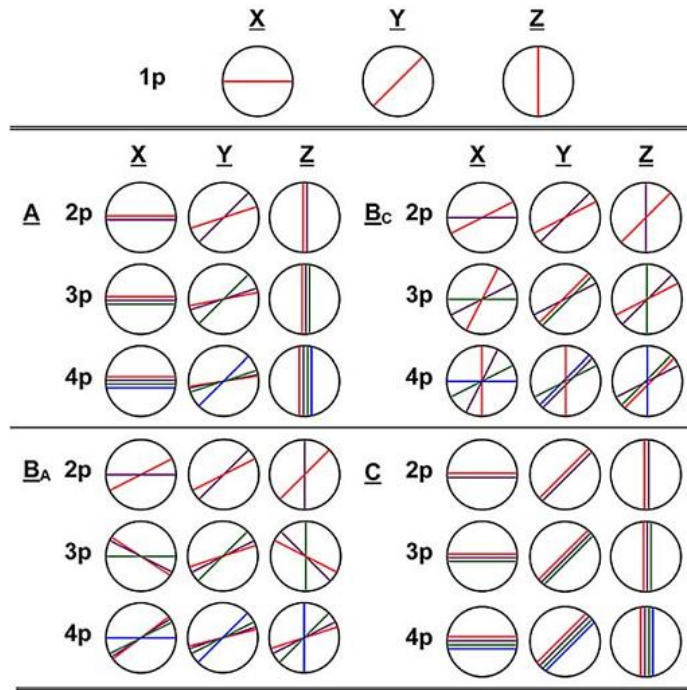
d. **Shearing Patterns**

Shearing pattern varies with processing routes. In route C, the shearing occurs on the same plane but the direction of shear is reversed between two consecutive passes. Thus, route C is expressed as a redundant strain process and the strain is restored after every even number of passes. Route B_C is also a redundant strain process as strain is cancelled at every two passes. But route A and B_A are not redundant strain processes. In route A, there are two shearing planes intersecting at an angle of 90° but in route B_A there are four planes intersecting at 120° angles. There is a cumulative build-up of additional strain on each separate pass.

The above distributions on X, Y, Z cubic planes are shown in Figure 1.8. The cubic element is restored every 2 passes using route C and every 4 passes using route B_C whereas more severe deformation takes place in case of routes A and B_A. Furthermore, there is no deformation of the cubic element on the Z plane when using routes A and C. In addition there is no distortion on Z plane in case of route A and C. In route B_A, non uniform deformation of X, Y, Z planes takes place whereas, in route B_C all planes (X, Y, Z planes) are getting deformed and amount of deformation varies with number of passes. Therefore, more uniform structure is expected in an ECAPed billet if route Bc is adopted.

Figure 1.8: The distortions of cubic elements on the X, Y and Z planes of sample for A, B_A, B_C and C processing routes [Furukawa et al. 1998].

Shearing patterns for $\Phi=90°$ and $\psi=0°$ can be seen in Figure 1.9. The shearing angle of all planes (X, Y, Z) is zero in case of route C but it is zero only for X and Z planes in route A. Thus, the angular range is zero on all planes when using route C or when viewing the X or Z planes in route A. The angular measurement of shearing planes in case of route Bc suggest that largest angular range of 90°, 63° and 63° after 4 passes of ECAP are achieved on the X, Y and Z planes, respectively.

Figure 1.9: The shearing patterns on the X, Y and Z planes for processing routes A, B_A, B_C and C: mauve, green and blue colors correspond to the 1, 2, 3, 4 pass, respectively [Furukawa et al. 2002].

1.3.6   Rotary-Die ECAP

It is a simple procedure to eliminate need of removing specimen from the die between each pass (Figure 1.10). The facility consists of a die containing the two channels of same cross section intersecting at the centre of the die at an angle of 90°. Sample is inserted in the vertical channel and three punches of equal length are inserted in the opposite ends. Now an upper punch is inserted in the vertical section to press the sample. The die is rotated by 90° to press the sample again. In this process sample is pressed using route A without any rotation. This technique has been used [(Ma, Suzuki, Saito, et al., 2005, Ma, Suzuki, Nishida, et al., 2005] for ECAP of hypereutectic Al–23 mass% Si alloy for 32 passes at the high temperatures of 673 K and 623 K and absorbed energy was measured by Charpy test. Absorbed ene9rgy got increased significantly with increasing the number of passes, ultimately reaching 13 kJ/m^2 after 32 passes. The grains got fragmented to less than 150 nm [Ma, Suzuki,

Nishida, et al., 2005]. A disadvantage of this process is small aspect ratio of samples and consequently significant inhomogeneity of microstructure [Valiev et al. 2006].
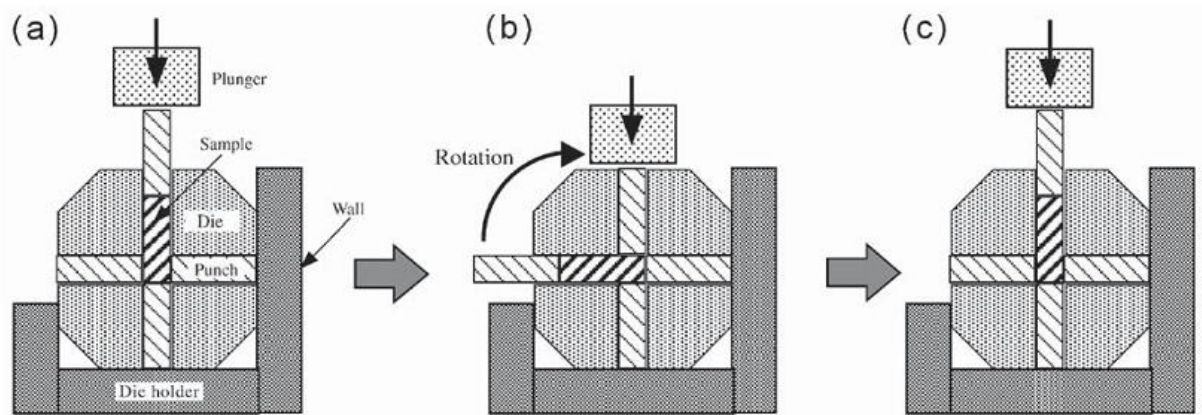
Figure 1.10: Geometry and operation of Rotary-Die ECAP (initial state) (b) after one pass (c) after 90° die rotation [Valiev et al. 2006].

1.3.7 Side Extrusion ECAP

This is an alternative approach in which high forces are applied by four punch-pull cams (Figure 1.11). Sample is pressed alternatively by punch B and punch A under a perpendicular pressure as shown in Fig. 1.11 [Valiev et al. 2006]. This process is similar to route A and ultra low carbon steel has been deformed by side extrusion ECAP upto 10 passes that resulted in refinement to 0.5µmX0.2µm and the tensile strength got increased to 1000 MPa [Azushima et al. 2002].
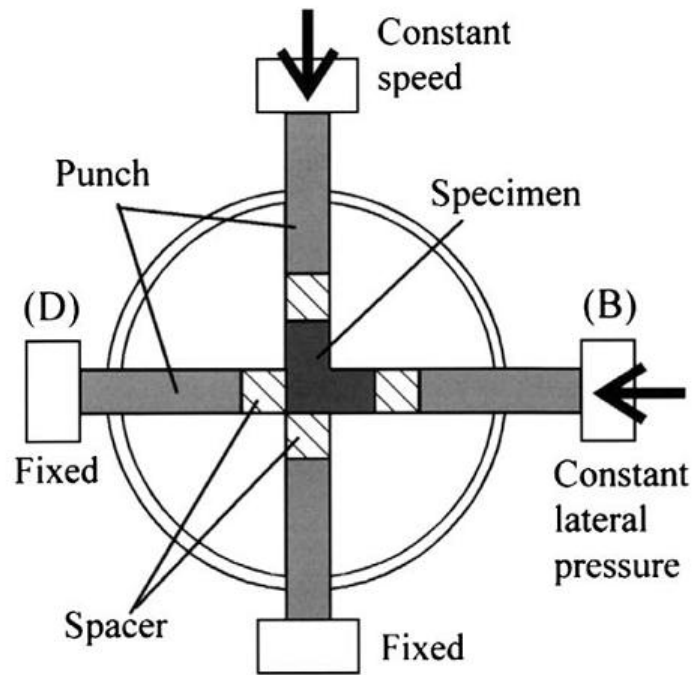
Figure 1.11: A schematic diagram of side extrusion process for ECAP [Valiev et al. 2006].

1.3.8   ECAP with Parallel Channel

In this new approach two parallel channels are used for two distinctive events to take place which results in reduction in number of passes for the formation of ultrafine-grained structure. K is displacement between two channels and Φ is angle of intersection between channels (Figure 1.12). In the schematic diagram of ECAP with parallel channels N shows shearing direction and the internal shaded region represent the shearing as the sample pass through the shearing zone. In this processing, uniform strain distribution is observed in the pressed sample even in the tail region when the Al sample is pressed upto 8 passes [Raab et al. 2005]. Strength of Al got increased from 71 MPa to 180 MPa by refinement of grain size to 0.6-1.1 μm.
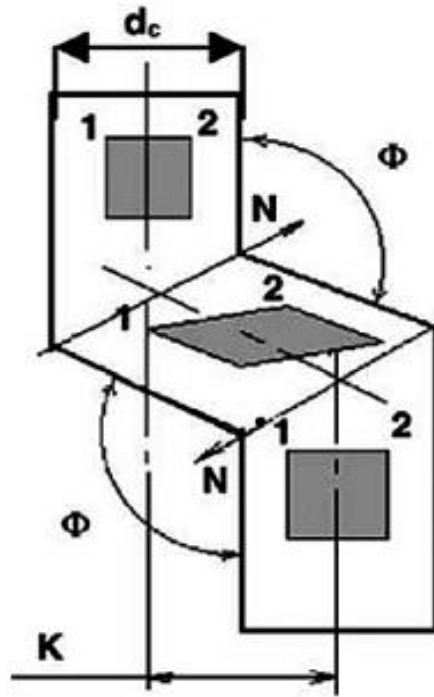
Figure 1.12: A schematic illustration of principle of ECAP with parallel channels [Raab 2005].

1.3.9 Multi Pass ECAP

In this process a die is constructed having multiple pass channels separated at an angle of 90° (Figure 1.13). In subsequent passes sample is rotated by 180° so that this process is equivalent to route C. Positions 1,2,3,4,5 corresponds to 1,2,3,4,5 number of passes [Nakashima et al. 2000]. Multi pass ECAE of low carbon steel refine the material from 20 μm to 6.7 μm and results in strengthening the material from 376 MPa to 718 MPa and elongation from 41.2% to 10% [Hwang et al. 2015].
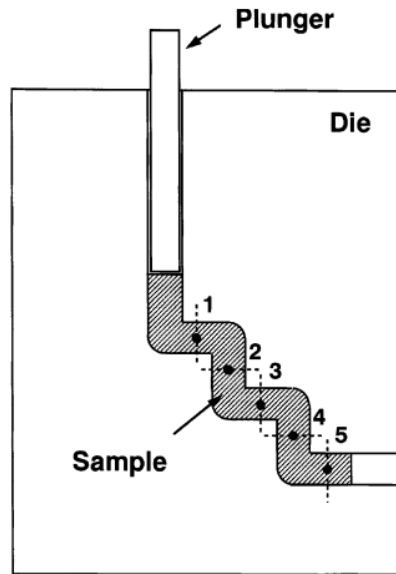
Figure 1.13: A schematic representation of a multi-pass facility for ECAP [Nakashima et al. 2000].

1.3.10 Drawbacks of ECAP

The primary drawback of the ECAP process is a considerable amount of material at the leading and trailing end of work piece. The length of the work piece is limited because very large frictional stresses can develop in the entrance channel. This imposes high stresses on the dies, which may fracture at points of stress concentration. Segal et al. [Segal 1995] and Semiatin et al. [Semiatin et al. 1999] have reported the problem of the high frictional forces in which the floor of the exit channel moved along with the work piece. For long rods large force is required to press the billet. However, due to elastic effects and lateral expansion of billet, high frictional forces are developed between work piece and the die. Billet of length 150 mm and 50 mm^2 diameter is the largest billet processed by ECAP process at the U.S Air Force Research Laboratory (AFRL) [Srinivasan et al. 2006].

1.4 Microstructural Development by ECAP

Microstructural refinement by SPD processes are extensively investigated for aluminium alloys, copper alloys and IF steel. Evolution of dislocation structures are discussed for fcc metals [Hughes 2001, Prangnell et al. 2004, Chang et al. 2000].

26

Grain refining mechanisms are summarised for fcc materials, mainly aluminium alloys, upto ε_{vm}= 10 by many groups [Hughes 2001, Prangnell et al. 2004, Chang et al. 2000, Furukawa et al. 1998].

Hughes et al. [Hughes et al. 2001] have reported homologous evolution of the deformation microstructure from small to large strains during SPD. Cells are basic units of microstructure. Cell boundaries are made of incidental dislocation boundaries (IDBs) and compose blocks of cells surrounded by geometrically necessary boundaries (GNBs). Prangnell et al. [Prangnell et al. 2004] have reported that coarse grains subdivide into primary deformation bands. There is a formation of aligned cell blocks within bands containing incidental dislocation boundaries, geometrically necessary boundaries and Taylor lattices at ε_{vm}<2. At ε_{vm}=2-4, already formed high angle grain boundaries (HAGBs) get aligned in the direction of deformation to form lamellar structures. Spacing of lamellar boundaries decrease to one or two subgrain wide as strain increases to ε_{vm}=4-6. When lamellar width decreases to one or two subgrain wide, the elongated bands take the shape of ribbon. Aspect ratio of ribbon grains increase further at ε_{vm}=5. At ε>6, ribbon grains break up by rotation of subgrains due to inhomogeneous plastic flow induced by texture and rate of grain refinement slows down and ribbon grains get shortened by formation of the transverse LAGBs. Ribbon grains get subdivided by specific transverse boundaries into submicrometer grains. Chang et al. [Chang et al. 2000] have reported transformation of polygonized dislocation walls into partially transformed boundaries and then into grain boundaries by dissociation of lattice dislocations. Grain refinement mechanisms operative during ECAP of commercial purity aluminum at room temperature are explored by Manna et al.. They found that banding takes place at initial passes. The degree of grain refinement is also highest during this stage. Increasing number of

ECAP passes (ε_{vm}=0.6-3.6) leads to elongation of grains by simple shear deformation, subdivision of grains to bands and subgrain formation in bands. Bands get fragmented into grains by intersection of bands as billet is rotated after every pass (ε_{vm}=1.2-2.4). Finally at large equivalent strain subgrains get converted into grains by continuous dynamic recrystallization process of progressive lattice rotation [Manna et al. 2012]. During accumulative roll bonding of IF steel grain size refines with increasing strain without saturation to a value 90 nm at an ε_{vm}= 8 [Hansen et al. 2009]. ECAP of IF produces banded structures and band remains till 8 passes [Branislav et al. 2007]. Chen et al. [Chen et al. 2003] discuss the microstructure evolution of IF steel during cold rolling at strain of $\leq$ 9.8%. The grain boundaries obtained by severe plastic deformation are non-equilibrium in nature and contain disordered dislocation network [Hansen 2001].

Various IF steels have been deformed by ECAP upto maximum equivalent strain of 9.2 and achieved a microstructural refinement upto 200 to 300 nm [Purcek et al. 2012, Saray et al. 2013, Kim et al. 2005, Gazder et al. 2008, Krajňák et al. 2013, Hazra et al. 2011, Máthis et al. 2011, Gazder et al. 2011, Messemaeker et al. 2005]. Hazra et al. [Hazra (a) et al. 2011] have processed IF steel to an equivalent strain of 9.2 and reported boundary spacing of 272 nm. At equivalent strain 9.2, the microstructure consists of elongated subgrains and grains aligned along the direction of imposed negative simple shear as well as some fraction of equiaxed subgrains/grains. Saray et al. [Saray et al. 2011] have deformed IF steel by Equal-channel sheet extrusion (ECASE) process and reported micro shear bands in the interior of grains with high density of dislocations. Deforming IF steel at equivalent strain of 9.2 resulted in equiaxed grains with relatively higher dislocation density and grain size of 240 nm [Purcek et al. 2012]. Saray et al. [Saray et al. 2013] have

reported equiaxed grain formation due to intersection of shear planes during 90°
rotation of billet between repetitive passes of ECAP process.

The microstructural refinement is dependent on composition of steel [Purcek
et al. 2012, Saray et al. 2013, Kim et al. 2005], amount of strain, type of routes as well
as geometry of the die [Valiev 2006]. Degree of refinement in IF steel increases with
increasing carbon content [Purcek et al. 2012, Saray et al. 2013, Kim et al. 2005,
Gazder et al. 2008, Máthis et al. 2011], amount of total equivalent strain [Gazder et al.
2008, Li et al. 2006, Hazra et al. 2009, Hazra et al. 2011], amount of equivalent strain
per pass or increasing of severity or decreasing intersection angles [Li et al. 2007].
Among all, amount of strain has strong effect on microstructural modification.

1.5 Texture of Ultrafine-Grained Materials

When a polycrystalline material has nonrandom orientations of grains,
material is called textured or has preferred orientation [Hu 1974]. Texture can be
changed by important processing techniques such annealing, deformation,
solidification and phase transformation. Deformation texture is described by
{hkl}<uvw> notation where {hkl} plane lies parallel to the rolling plane and an
direction <uvw> lies parallel to the rolling direction [Hu 1974]. In case of rolling
certain crystallographic planes are aligned parallel to rolling plane and particular
directions in these planes are parallel to rolling directions. Whereas, shearing texture
tend to have preferred planes {hkl} parallel to shearing plane and preferred direction
<uvw> parallel to shearing direction. Texture is inhomogeneous in processes such as
forging, deep drawing etc. and nature of stress varies from place to place due to
friction between sheet and surface. Texture developed at surface is shear or inverse
shear texture while at the centre it is plane strain texture. Texture resulted from SPD
processes give rise to plastic anisotropy [Alexander et al. 2005, Han et al. 2003,

Beyerlein et al. 2007, Yapici et al. 2007, Yapici et al. 2009]. Study of texture is necessary as properties of materials such as strength, work hardening, plastic anisotropy; formability, grain refinement and fracture are affected by deformation texture. Texture or anisotropic mechanical behaviour is necessary for better control on designing and energy efficiency [Beyerlein et al. 2009].

Annealing texture is different from deformation texture. During annealing, initial stage of recovery occurs by thermally activated movement of opposite sign dislocations and rearrangement of same sign dislocations along a boundary called low angle grain boundaries or cells but no change in texture takes place. During recrystallization new grains nucleate and grow at the expense of cold worked matrix by migration of high angle grain boundaries. There can be components of texture common to both deformed and recrystallized states. Grain growth takes place by gradual grain boundary movement and leads to change of texture [Humphreys 1995]. Texture can be represented by pole figures (PFs) or stereographic projections of particular direction of crystal on sample reference axes, inverse pole figure or orientation of sample axis or direction (ND, RD or TD) on crystal axis and orientation distribution function (ODFs) on Euler space or orientation space.
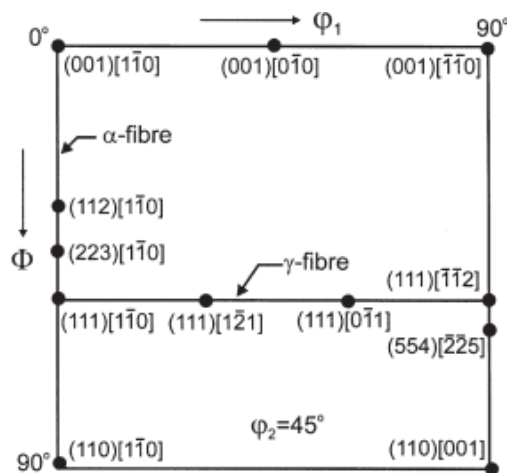
1.5.1 Fiber Texture

In fiber texture one or two specific crystallographic directions are oriented parallel to wire or rod axis whereas, other crystallographic directions are oriented more or less randomly around the axis [Hu 1974]. Fiber texture is developed during drawing, swaging, rod-rolling, or extrusion of wires and rods. If preferred orientation is developed in radial direction it is called cyclic texture. The preferred orientations of metal depend mainly upon the crystal structure of the metal. For cubic (fcc and bcc)

metals or alloys, a [100] direction is usually parallel to the long axis of grains, other crystallographic axes are oriented at random around this [100] direction.

a. Rolling and Recrystallization Texture

The rolling and recrystallization textures of bcc metals are usually described by two fibre components (Figure 1.14): (1) partial α-fibre with <110> direction parallel to the rolling direction and (2) γ fibre with <111> axis parallel to the normal direction [Kohler et al. 1995]. Partial α-fibre contains {001}<110>, {112}<110> and {111}<110> orientations. Partial γ fibre includes the {111}<110> (common to both fibres) and {111}<112> orientations. With increasing deformation the rolling texture changes in a characteristic way, considering the main components: the orientations {001}<110> to {111}<110> increase gradually for high degrees of deformation while the {111}<112> orientation shows strong increase of intensity upto 50% deformation and remains constant with further rolling. At high degree of deformation, maxima are observed at the orientations {112}<110> or {111}<110> [Kohler et al.1995]. Main components of rolling texture are {001}<110>, {112}<110>, {111}<110>, {111}<112> and {11,11,8}<4,4,11>.

Figure 1.14: Position of important texture components in BCC materials [Humphreys et al. 1995, Hutchinson 1999].

The main ideal orientations and fiber textures in rolling shear of bcc materials are listed in Table 1.2 [Suwas et al. 2008].

At the initial stage of recrystallization process in α-iron, there is an increase of intensity of orientation of {001}<110> to {112}<110> components. Whereas, the orientation density for γ fiber is low. With further annealing, orientation density of {001}<110> to {112}<110> decreases but density of {111}<110> remains constant while density of {111}<112> becomes stronger. After complete recrystallization strong γ fiber forms with maxima at orientation {111}<112> [Emren et al. 1986].

1.5.2 Ideal Texture in Simple Shear Deformation of BCC Material

Based on modelling of torsion test, main ideal orientations and fiber textures in simple shear of bcc materials are shown in Table I.1.

Table 1.1: Ideal orientations in simple shear in BCC materials [Beyerlein et al. 2005, Li et al. 2005].

| Sl.No.		{hkl}<uvw>	φ_1, (°)	Φ, (°)	φ_2, (°)
1	$D_{1\theta}$	$(\bar{1}\bar{1}2)[111]$	54.74/234.74 144.74	45 90	0/90 45
2	$D_{2\theta}$	$(11\bar{2})[111]$	125.26 35.26/215.26	45 90	0/90 45
3	E_θ	$(110)[1\bar{1}1]$	90	35.26	45
4	$\bar{E}_\theta$	$(\bar{1}\bar{1}0)[\bar{1}1\bar{1}]$	270	35.26	45
5	J_θ	$(110)[1\bar{1}2]$	90/210	54.74	45
6	$\bar{J}_\theta$	$(\bar{1}\bar{1}0)[\bar{1}12]$	30/150/270	54.74	45
7	F_θ	$(110)[001]$	0/180 90/270	45 90	0/90 45

Table 1.2: Main ideal orientations of rolling texture of bcc materials [Suwas et al. 2008].

{hkl} <uvw>	ϕ_1	ϕ	ϕ_2
{001} <110>	45	0	0
{211} <011>	51	66	63
{111} <011>	60	55	45
{111} <112>	90	55	45
{11,11,8} <4,4,11>	90	63	45
{110} <110>	0	90	45

Figure 1.11 is ideal ECAE simple shear model texture for negative simple shear. It depicts partial <111> fiber (denoted as $<111>_\theta$) and {110}-fiber (denoted as ${110}_\theta$) that are CCW (counter clock wise) rotated around transverse direction (TD) for θ~60° for Φ=120°. $<111>_\theta$ fiber contains $D_{2\theta}$, $E_\theta/\bar{E}_\theta$ texture components and the ${110}_\theta$ fiber contains $E_\theta/\bar{E}_\theta$, $J_\theta/\bar{J}_\theta$ and F_θ orientations the $E_\theta/\bar{E}_\theta$ components are common to both fibers [Beyerlein et al. 2005].

During multi pass ECAP process where simple shear takes place, sample is rotated around TD axis. This TD is axis of symmetry of simple shear process. For routes A and C, TD is called texture symmetry axis. Monoclinic symmetry exists around this axis for routes A and C [Gholinia et al. 2000, Li et al. 2007, Li et al. 2006]. In route C, every pass reveres the shear direction whereas plane of shearing remains same. Even number of passes reveal initial texture while odd number of passes reveals first pass texture [Li et al. 2007, Li et al. 2006, Ferrasse et al. 2004]. Whereas, in routes B_A and Bc texture is rotated between passes around an axis which

is not the axis of symmetry of the process. Thus, monoclinic symmetry is lost in this process [Beyerlein et al. 2009].
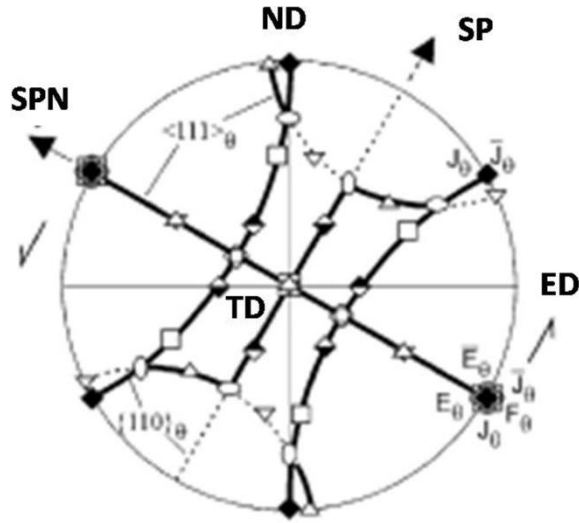
Figure 1.15: (110) pole figure showing the locations of the corresponding main ideal orientations ($D_{1\theta}$, $D_{2\theta}$, E_θ /$\bar{E}_\theta$, J_θ/$\bar{J}_\theta$, and F_θ) and fiber textures (<111>$_\theta$ and {110}$_\theta$) derived from negative simple shear by a 60° CCW-rotation around the z-axis. Contour levels:1/1.4/2/2.8/4/5.6 [Beyerlein et al. 2005].

Ideal orientations for BCC material is simple shear texture. There are two fibers formed during simple shear deformation (1) alpha fiber {110}<uvw> and (2) Gamma fiber {hkl} <111> [Gholinia et al. 2000]. D_1/D_2 and $E/\bar{E}$ are components of gamma fiber and $J/\bar{J}$ are components of alpha fiber. Ideal orientations are F, J, $\bar{J}$, E, and $\bar{E}$ with weak D_1 [Beyerlein et al. 2009]. In negative simple shear of ECAE process, the D_1 component is weak [Beyerlein et al. 2009, Baczynski et al.1996, Li et al. 2005].

1.5.3 Texture of IF Steel

Jin et al. have reported increase in intensity of deformation texture with number of continuous confined strip shearing passes (upto ε_{vm}=1.98) due to development of deformation texture or rotation of grains to one stable orientation [Jin et al. 2004]. They have reported vanishing γ-fiber orientations of the initial sample and the texture maximum is reported at (122) [$\bar{6}$21] and (211)[$2\bar{6}$1] orientations. Li et

al. have reported texture development by ECAP process upto ε_{vm}=4.6 using routes A, B_A, C, Bc. They have reported that there is more rapid refinement after ε_{vm}=2.3 in route C and after ε_{vm}=4.6 in route Bc. They have concluded that texture development with deformation is gradual process because of unidirectional rotation of billets about extrusion direction (ED) and more uniformity of alpha and gamma fibers in routes A and C than in routes B_A and B_C. They have got the primary texture components to be located between $D_{1\theta}$ (TT2)[111] and E_θ (TT0)[T1T] and a tendency of orientation flow from E_θ to $D_{1\theta}$ with an increase in number of passes [Li et al. 2006]. Gazder et al. have reported on the basis of ODF maps that at ε_{vm}=1.15, J1 (35/215, 45, 0) (125/305, 90, 45), J2 (145/325, 45, 0) (55/235, 90, 45) components are prominent. These remain unchanged at ε_{vm}=2.3-4.6 but their intensity and spread gets changed [Gazder et al. 2006]. Messemaeker et al. have done ECAP upto ε_{vm}≈4.6 and on the basis of ODF maps found that intensity is evenly distributed at ε_{vm}=1.15 while it varies along its length at ε_{vm}=2.3. They have reported J1 (30, 54.7, 45) and J2 (90, 54.7, 45) as most important components at ε_{vm}=4.6 [Messemaeker et al. 2005]. Bhowmik et al. have ECAPed IF steel upto ε_{vm}≈4.6 and reported evolution of partial <111> and {110} fibers after ε_{vm}=1.17 and gradual decrease in intensity of texture components after ε_{vm}=4.68 [Bhowmik et al. 2009]. Pereloma et al. have reported on the basis of pole figure maps that torsion components rotate away from their ideal position at mid cycle (ε_{vm}=1.32-1.98 and 3.3-4.62) and come to exact position at high strain levels (ε_{vm}=5.28). The principle slip direction of crystal aligns with shear direction with increased number of passes [Pereloma et al. 2005]. Hazra et al. [Hazra(a) et al. 2011] have discussed microtexture (ECAPed upto ε_{vm}=9.2) and got primary components to be located along <111> partial fiber between $D_{1\theta}$ and $E_\theta/\overline{E_\theta}$ components along with weak {110} fibers. Li et al. [Li et al. 2007] have reported that primary texture (at

ε_{vm}=0.67) is located along $D_{1\Theta}$ (114.74/294.74, 45, 0) (24.74/204.74, 90, 45) or <111>$_\Theta$ fiber which gets weakened beyond ε_{vm}=1.34, whereas, after ε_{vm}=2.68, primary components get located between $D_{1\Theta}$ to E_Θ (150, 35.26, 45)/$\overline{E_\Theta}$ (330, 35.26, 45) along <111>$_\Theta$ fiber [Li et al. 2007]. Initially deformation takes place by formation of dislocations and maximum strengthening is provided by LAGBs, contribution of strengthening by HAGBs takes place at high strain level (ε_{vm}≈9.2) [Gazder et al. 2008]. So far texture analysis of IF steels upto equivalent strain 9.2 has been reported [Magnusson et al. 2001, Zhu et al. 2000, Pereloma et al. 2005, Jin et al. 2004, Li et al. 2006, Hazra et al. 2009, Li et al. 2007, Bhowmik et al. 2009, Gazder et al. 2008, Gazder et al. 2006, Messemaeker et al. 2005]. Therefore texture is important in SPD processes under large strains and strain path as well.

Texture strength is maximum intensity level of texture normalized by random. It is measured by texture index T as

$$T = \int [f(g)]^2 dg \tag{1.14}$$

Where f(g) is orientation density function and g(φ1.φ,φ2) is orientation defined by Euler angles. Li et al. [Li and Alexander et al. 2005] have shown that texture strength increases with pass number in ECAE process of Cu. Opposite trend is also observed in Cu as texture strength got weakened with pass number in route Bc of ECAE process [Baik et al. 2003].

1.6 Strengthening Mechanisms

To strengthen the material, simple method is to introduce huge amount of dislocations to prohibit movement of dislocations. There are many processes which hinder dislocation motion. These are work hardening, grain boundary hardening, precipitation hardening, dispersion hardening and solid solution hardening. Among all

these methods work hardening and grain boundary hardening are mainly responsible for increasing strength of UFG IF steel [Purcek, Saray, Nagimov et al. 2012].

1.6.1. Work Hardening

When mobile dislocations interact with other dislocations, dislocations themselves become obstacles to dislocation motion. Thus, the glide resistance for dislocations increases and results in work hardening. When the mobile dislocations run into the immobile dislocations, it is pinned by the immobile ones until the applied resolved shear stress overcomes the obstacle strength, τ_{ob} given by

$$\tau_{ob} = \alpha \frac{Gb}{L} \tag{1.15}$$

Where α is a factor giving obstacle strength, L is mean spacing of dislocations and G is shear modulus of matrix and b is Burger vector.

Plastic flow occurs in metals when applied resolved shear stress (τ) equals to the obstacle strength (τ_{ob}). This means that during plastic flow, the flow stress will have to be

$$\tau = \alpha G b \sqrt{\rho} \tag{1.16}$$

Where ρ is dislocation density $\rho = 1/L^2$.

The tensile stress (σ) is used and the above relationship is expressed by

$$\sigma = \sigma_o + \alpha G b \sqrt{\rho} \tag{1.17}$$

Equ. 1.9 describes the relationship between flow stress and tensile stress. Where σ_o is the intrinsic lattice strength. Dislocations gliding on intersecting planes impede dislocation motion and high strain hardening is achieved. The reason for this strengthening is supposed to be interaction of stress field of dislocations [Zbib et al. 2002, Weihnacht et al. 2001], interpenetration of one slip system into other (dislocation jogs) and formation of sessile jogs [Dieter 1986].

1.6.2 Grain Boundary Strengthening

Grain boundaries in a polycrystalline material act as barriers to dislocation motion. Grain boundaries are planar defects and are stronger obstacles to dislocation motion than linear defects or point defects because the dislocation pinning is along the entire length of the dislocation line that intersects the boundary. Due to orientation difference across grain boundary, passage of dislocation motion to the adjacent grain is blocked. In a polycrystalline material the grain size can be correlated to yield strength by the so called Hall-Petch relation [Callister et al. 2001]

$$\sigma_y = \sigma_0 + k\, d^{-1/2} \qquad\qquad\qquad (1.18)$$

Where k is a material constant and σ_o is the intrinsic lattice strength and d is grain size.

1.7 Properties of Ultrafine-Grained Materials

Ultrafine-grained materials produced by SPD posses attractive properties of high strength and hardness at low temperatures (Hall-Petch effect), improved formability at elevated temperatures. Mechanical properties of SPD materials improve several times over this normal condition due to change in grain size and shape, lattice defects in the grain interior, grain-boundary structure, fraction of low and high angle grain boundaries and the presence of segregations and second-phase particles. At different strain level different transport mechanisms take place which are also responsible for a variety of mechanical properties such as grain boundary diffusion, sliding or intragranular deformation. Now a days SPD nanomaterials are going over new direction of engineering multifunctional materials. SPD materials can have multifunctional properties like extraordinary combination of very high mechanical and functional properties including superelasticity and a shape memory effect in nanostructural TiNi alloy [Pushin et al. 2004]. Another example of multifunctional

material is Fe-Co which contains soft magnetic properties through interaction of magnetic moments across the grain boundaries in SPD processing [Vorhauer et al. 2004]. SPD nano structured materials can be applied in aerospace, transportation, medical devices, sports products, food and chemical processing, electronics and defence applications for nanomaterials [Valiev 2013, RZ Valiev 2006]. There is growing attention to the economically feasible continuous production methods for the processing of UFG materials [R.Z. Valiev 2006, Lowe 2006, Raab et al. 2004]. Nanostructural Ti long rods of 800 mm and diameter of 6.5 mm synthesized by ECAP followed by thermomechanical treatments with yield strength of 1100 MPa, ultimate tensile strength (UTS) of 1230 MPa and 14% elongation to failure. Applications of UFG materials include weight sensitive products like high performance mountain bicycles and automotive applications [Zhu et al. 2004]. New downscaling SPD processing technique is introduced by Estrin et al. who made porous steel preform with aluminium under imposed pressure through mm scale die [Estrin et al.2005].

Generally it is observed that IF steel containing 0.004wt% C can be strengthened from yield strength of 106 ± 10 MPa to 687 ± 9 MPa and ultimate tensile strength from 232 ± 13 MPa to 750 ± 6 MPa through ECAP by imposing an equivalent strain of 9.2. However ductility of the material drops down from total elongation of 53 ± 1 % to 14.7 ± 1.5 % and uniform elongation from $25\pm1\%$ to $1.8\pm0.3\%$ [Purcek et al. 2012, Saray et al. 2013, Saray et al. 2012]. The increase in strength is due to significant grain refinement, increase in dislocation density and substructure strengthening whereas the loss in ductility is due to decreased strain hardening capacity [Manna et al. 2012]. Even though ECAP of coarse grained IF steel reduces ductility but improvement in impact toughness, decrease in ductile-brittle transition temperature and suppression of cleavage fracture are observed on ECAPed IF steel,

[Saray et al. 2012]. Saray et al. have found improvement in impact toughness in terms of increment in charpy energy from ~8 J to ~9.5 J, reduction in ductile-brittle transition temperature from -40ºC to -90ºC and suppression of cleavage fracture, i.e. even not complete brittle fracture at -170ºC.

Table 1.3: Microstructure and mechanical properties of IF steels processed by SPD techniques.

| Year	Steel	Processing	Equivalent Strain	Grain size (nm)	Author	T.E. (%)	U.T.S. (MPa)	Hardness
2011	IF	ECAP	9.2	272	Hazra(a) et al. 2011	7.3	689	-
2010	IF	ECASE	9.2	-	Saray et al. 2010	11.4	528	163
2011	IF	ECASE	5.2	-	Saray et al. 2011	9.7	499	-
2011	IF	ECAP	9.2	66	Máthis et al. 2011	15%	850	290 HV
2012	IF	ECAP	9.2	240	Purcek et al. 2012	15%	748	-
2013	IF	ECAP	9.2	240	Saray et al. 2013	14.7	750	-
2002	IF	ARB	4	200	Tsuji et al. 2002	0.5	819	-
2009	IF	ARB	8	100	Hansen et al. 2009	<4	1032	-
1999	IF	ARB	4	-	Saito et al. 1999	6	751	-
2014	IF	ARB	8	<500	Tamimi et al. 2014	-	-	240 HV
1999	IF	ARB	5.6	420	N. Tsuji et al. 1999	9	870	-
2011	LCS	ECAP	3	300	Kraus et al. 2011	11.5	884	-
2002	LCS	ECAP	3	200	Fukuda et al. 2002	0.4	800	-

Ultra high strength and high ductility are essential requirements for steels to save weight and to be used for structural applications. Strengthening of steels of low carbon content through grain refinement can be achieved by thermomechanical treatment due to limitation in refinement to 4-5 µm level [Segal 2004]. Ultra high

strength can be achieved by grain refinement to ultrafine level through ECAP, which is an order of magnitude higher than that of thermomechanical treatment. Song et al. [Song et al. 2006] reviewed that grain size of low carbon steel can be reduced from 150 μm to ultrafine level of 200-300 nm and can be strengthened by 4-5 times (Figure 1.16) than that of coarse grained material. Therefore, yield strength of coarse grained (50 μm) material can be increased to ~1000MPa by refining (to 200-300 nm) it through various SPD processes. However, ductility of the material behaves differently as the grain size decreases in micron range. The ductility (both uniform elongation and total elongation) (Figure 1.17) increases in coarse grained condition but in the UFG range ductility decreases as the grain decreases due to lack of strain hardening or plastic instability. However, maximum ductility can be retained when grain size is in range 1-5μm (Figure 1.17) [Song et al. 2006]. Because of low ductility, applications of ultrafine-grained materials as structural parts are yet to be realised even though strength enhancement by two to five times take place.
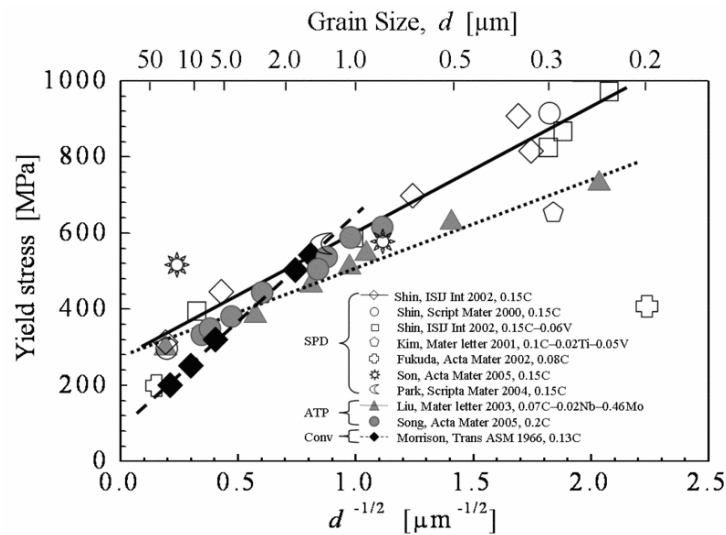
Figure 1.16: Variation of yield strength in low carbon steels with grain size from macrosize to ultrafine size for convensional to severe plastic deformation methods [Song et al. 2006].
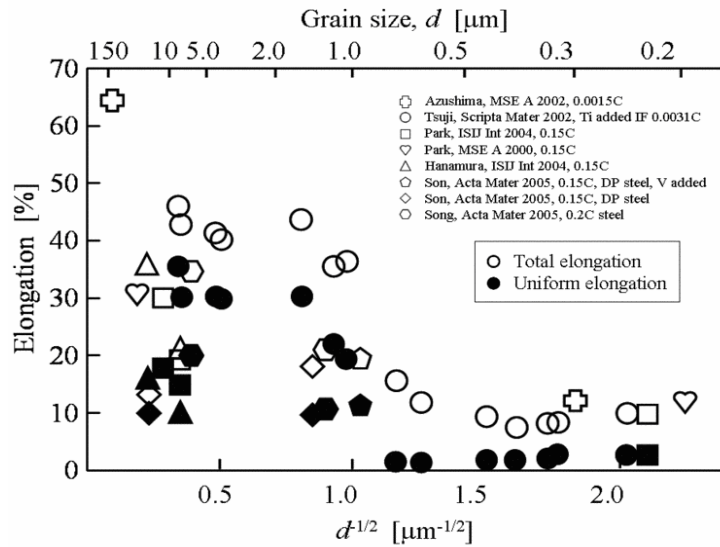
Figure 1.17: Variation of elongation in low carbon steels with grain size from macrosize to ultrafine grain size for convensional to severe plastic deformation methods [Song et al. 2006].

There are eight possible ways ductility of UFG/nanocrystalline materials can be recovered. These are incorporation of bimodal/multimodal) grain size distribution, a mixture of two or multi phases with varying size scales and properties, use of nano scale growth twins in lieu of the nano grains, strengthening by dispersion of nano precipitates, transformation induced plasticity (TRIP) and twining-induced plasticity (TWIP), lowering of dynamic recovery at low temperature (cryogenic temperature) and dynamic strain rate, improved strain rate hardening and synthesis of truely flaw free materials [Wang and Ma et al. 2004]. Except first one all others can be applied only for a specific alloy, however bimodal grain size distribution can possibly be applied for any polycrystalline metallic material. Wang et al. [Wang et al. 2002] have shown that bimodal grain size distribution is one of the processes to get desirable combination of high tensile strength and ductility where fine grains maintain strength and coarse grains allow dislocation activities or strain hardening there by ductility is comparable to coarse grained counterpart. Pure Cu is cold worked (93% thickness reduction) followed by annealing at 180ºC for 3 minutes. The material was partially

recrystallized. The microstructure consisted of vast majority of grains in nanocrystalline/ultrafine range with some recrystallized grains. As a consequence, it got yield strength 400 MPa (about 6 times higher than coarse grained pure copper) and elongation to fracture has less than about 5%. To further increase ductility deformed nanocrystalline Cu was annealed above secondary recrystallization temperarure at 200ºC for 3 minutes. The recrystallized grains produce well defined high angle boundaries and secondary recrystallization produces a significant volume fraction (around 25%) of coarser (1 to 3µm) grains. This process resulted in a bimodal grain size distribution with a few coarse grains together with many nanometric grains. As a result ~65% elongation to fracture and 30% uniform elongation were obtained. The ductility is thus comparable to that of annealed conventional grain size Cu, but the yield strength is ~ 7 times higher. [Barbosa et al. 2009].

Bimodal grain size distribution has been incorporated in Cu by thermo mechanical treatment with micro-metre-sized grains embedded inside a matrix of nanocrystalline and ultrafine (<300nm) grains (Figure 1.18, 1.19). Fine grains impart high strength whereas the inhomogeneous microstructure induces strain hardening that stabilize the tensile deformation, leading to a high tensile ductility 65% elongation to failure, and 30% uniform elongation [Wang et al. 2002].
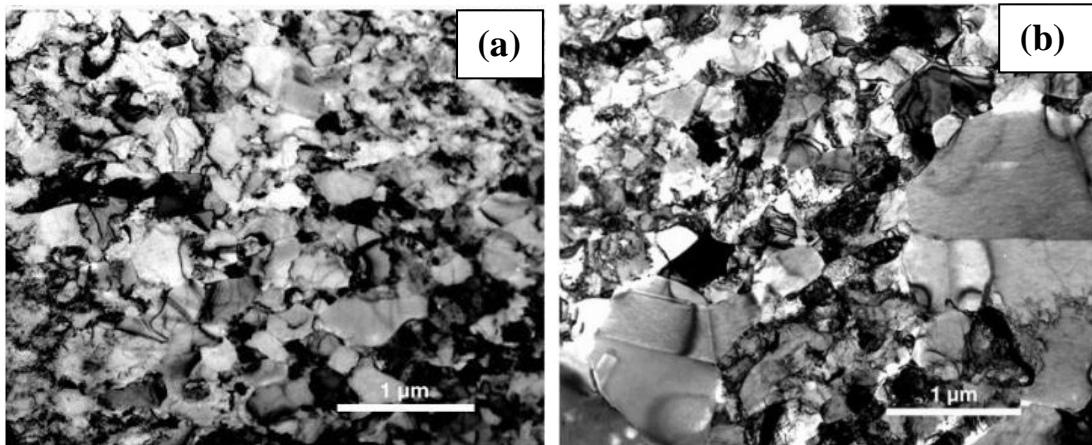
Figure 1.18: Transmission electron microscopy bright field image of (a) cold worked (at liquied nitrogen temperature) Cu after annealing at 180°C for 3 min (curve D in Fig. 1.15) (b) coldworked Cu after annealing at 200°C for 3 min (for curve E in Fig. 1.15). Major portion of the grains are in the nanocrystalline/ultra fine range with some recrystallized regions [Wang 2002].
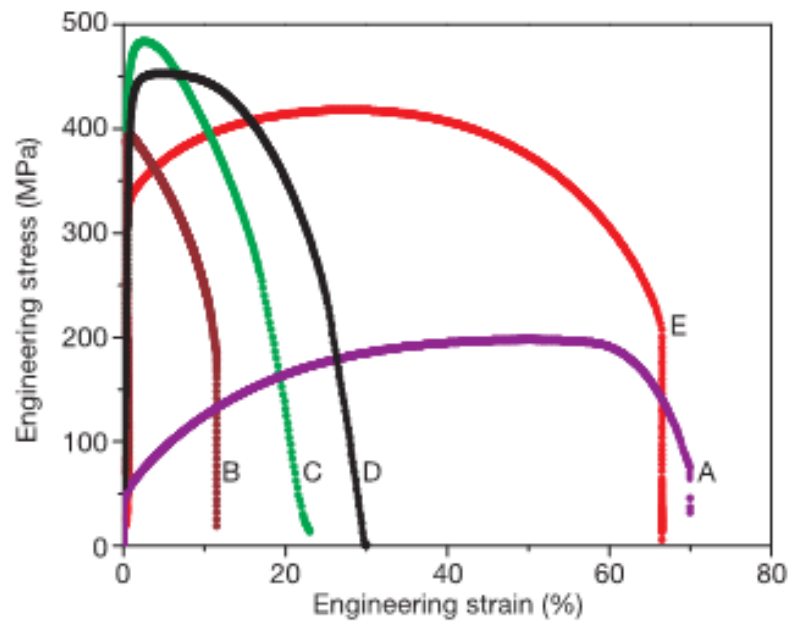
Figure 1.19: Engineering stress–strain curves for pure Cu. (A) annealed, coarse-grained Cu; (B) room temperature rolling to 95% cold work (CW); (C) liquid-nitrogen-temperature rolling to 93% CW; (D) 93% CW, 180°C) 3min and (E) 93% CW 200°C for 3 min [Wang 2002].

High density of nanoscale twins in Cu (prepared using electrodeposition) has reported a significant enhancement in flow strength, tensile strength, uniform plastic strain and work hardening rate [Delince et al. 2007]. Enhancement in ductility and strength in nanocrystalline Al where the second phase is uniformly distributed is due

to the increased dislocation accumulation and resistance to dislocation-slip. Here 7075 Al alloy is first solution-treated at 500°C for 5 h then quenched into liquid nitrogen (LN) to obtain a coarse-grained (CG) super saturated solid solution. This CG sample is immediately cryorolled to produce nanostructures (grain size 100 nm). The NS sample is then aged at low temperature to introduce very small second phase particles of 10 nm diameter and 4 nm thickness. By this method enhancement of uniform elongation is reported more than double [Sun et al. 2009].

Ductility can be enhanced by possible combination of two phases for limiting the mobility of dislocations and composite effect. A typically dual phase (ferrite-martensite) microstructure can be obtained in a steel of 0.15 wt% C, 1.7 wt% Mn, 0.5 wt% Si, 0.012 wt% Nb and balance Fe by the following steps. These are (i) cold swaging (i.e. rotative hammering technique which reduces the diameter of a bar by imposing a highly non-radial compressive loading path, involving a lot of redundant plastic strains), (ii) an optional homogenization annealing to produce larger grain size, (iii) an intercritical annealing at 730°C in a fluidized bed furnace and (iv) water quenching. This processing route has reported for three dual-phase microstructures with various ferrite grain sizes: coarse grains (CG), fine grains (FG) and very fine grains (VFG). A low carbon steel has been ECAPed in ferrite pearlite and martensite condition and submicron size grain structure is produced. Yield strength improved from 430MPa to 590MPa but ductility decreased from 10.3% to 5.8%. [Yoda et al. 2011].

A reduction in SFE can increases strength and tensile ductility. The effect of stacking fault energy (SFE) on the mechanical properties is reported in Ni–Co alloys which have minimum solution hardening effects. Cobalt reduces the SFE in nickel and promotes grain refinement during processing and increases the dislocation and

twin densities. The higher strength is due to grain refinement, higher dislocation and pre-existing twin densities whereas the higher ductility is attributed to a higher work hardening rate [Beyerlein 2009].

1.8 Abnormal Grain Growth

When deformed materials are annealed at very high temperature (above secondary recrystallization) for long duration a few grains grow at rapid rate and distribution of grain size changes from normal distribution to abnormal one, such grain growth is named abnormal grain growth or secondary recrystallization. Driving force for abnormal grain growth is reduction in grain boundary energy. If some material is annealed at low temperature normal grain growth process is inhibited but at elevated temperature case of inhibition is removed and a few grains grow at fast rate and consume most of the other. However if this elevated temperature annealing is applied for short duration, a few grains only grow to large one while most of the other is recrystallized but remain in refined condition. Texture, second phase particles and surface effects are the main factors for abnormal grain growth to occur [Humphreys et al. 1995]. Abnormal grain growth is characterized by bimodal grain size distribution. There are two predictions for nucleation limited coarsening:

First is that fast growing grains should completely consume slowly growing grains population and second is that during abnormal grain growth, density of small grains should decrease whereas large grains should remain constant [Rohrer et al. 2005]. Development of bimodal grain size distribution principle can be adopted to get ultra high strength and high ductility for steels for structural applications. Ultra high strength can be achieved by grain refinement to ultrafine level through ECAP. Unfortunately ductility of ultrafine-grained materials is much lower than that of their coarse counter part due to lack of strain hardening or plastic instability (Figure 1.16

and Figure 1.17) [Song et al. 2006]. Because of low ductility, applications of ultrafine-grained materials as structural parts are delayed. IF steel containing 0.004wt% C has been strengthened from yield strength of 106±10 MPa to 687±9 MPa and ultimate tensile strength from 232±13 MPa to 750±6 MPa by ECAP by giving an equivalent strain of 9.2. However ductility of the material drops down from total elongation of 53±1 % to 14.7±1.5 % and uniform elongation from 25±1% to 1.8±0.3% [Purcek 2012, Saray 2013, Saray 2012]. The increase in strength is due to significant grain refinement, increase in dislocation density and substructure strengthening whereas the loss in ductility is due to decreased strain hardening capacity [Manna et al. 2012]. Higher ductility of materials with micron sized (1-5 μm) grains can be achieved in steels by unit dislocation controlled plasticity and appreciable work hardening. Therefore, process parameters need to be controlled to produce bimodal/multimodal distribution in grain size where majority of grains are in ultrafine range which will maintain ultra high strength and a small amount of micron size grains that will provide required ductility that is controlled by slip and work hardening.

Bimodal grain size distribution has been reported by cold rolling of dual phase structures followed by annealing treatment of low carbon steel [Alizamini et al. 2007]. This method is based on fact that there is difference in the recrystallization behaviour of ferrite and martensite combined with carbide precipitation in the martensitic regions yields a heterogeneous microstructure with a distribution of coarse and fine grains. Steel of composition 0.17C, 0.74Mn, 0.04Al, 0.008P, 0.009S and 0.0047N (wt.%) is initially austenitized at 1000°C for 30min followed by rapid quenching into an ice brine solution to get martensite. The resulting martensite structure is then intercritically annealed in a salt bath at 740°C for 10 min followed by direct

quenching into an ice brine solution. The resulting ferrite/martensite dual phase structure is cold rolled by 50% reduction with a laboratory rolling mill, then annealed between 500-600°C for different times in Ar atmosphere before water quenching. Among different annealing conditions, holding at 525°C for 1200 min has been reported to offer an appropriate condition for developing a bimodal structure [Alizamini et al. 2007].

On intercritical rolling the development of any microstructure depends on the amount of deformation, the deformation temperature, strain rate and time. This concept is used to evolve bimodal grain size distribution in steel of chemical composition (in wt. %) 0.103 C, 0.490 Mn, 0.006 Si, 0.010 P, 0.014 S, 0.035 Al, and 0.0045 N. Rolling at intercritical temperature of 800°C, results in bimodal grain size distribution, the large grains are due to combination of transformation of deformed austenite into undeformed ferrite (transformation-induced (TI) nucleation of ferrite) and rapid undeformed ferrite grain growth into the deformed ferrite. The small grains in the bimodal grain size distribution are subgrains resulted from extensive recovery of deformed ferrite [Bodin et al. 2001].

Second phase particles act as pinning points for grain growth above limiting grain size. Hillet (1965) and Gladman (1966) have studied abnormal grain growth or discontinuous grain growth or secondary recrystallization by modelling [Hillert et al.1965, Gladman 1966]. The onset of abnormal grain growth is possible when there is inhomogeneous grain growth due to local destabilization of grain structure by weakening of critical pinning points. If material is having broad range of grain size distribution, nucleation of abnormal grain growth will be feasible. When normal grain growth is inhibited at low temperature, abnormal grain growth can take place. If material is annealed at very high temperature or long time after normal grain growth

stage. Abnormal grain growth occurs on further annealing of single strong textured fine grained recrystallized material as within a textured volume of grain boundaries there are grains having lower mean misorientation and low energy mobility than normal grain structure. If material is having grains of other texture components as well, there will be higher mean misorientation and migration of these boundaries like primary recrystallization. Diffused texture components contain many high angle grain boundaries (HAGBs) of average misorientation>15° and nuclei for discontinuous grain growth. In diffuse textured material abnormal grain growth will be easy but maximum size ratio of abnormally growing grain is small.
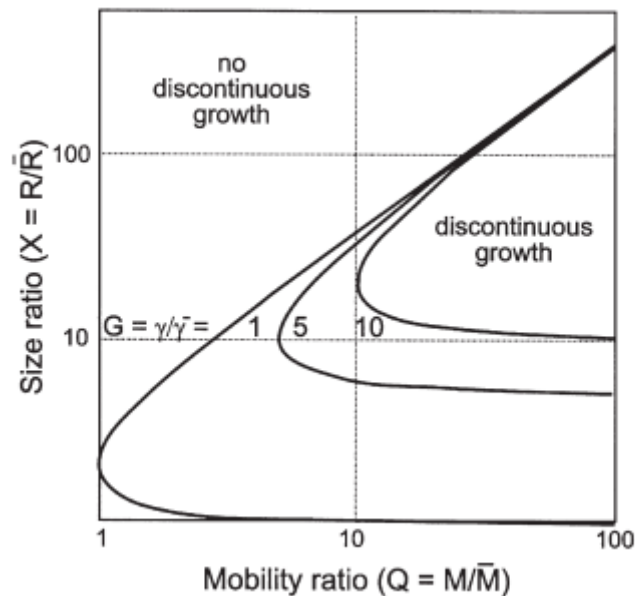
Figure 1.20: The conditions for discontinuous growth as a function of the relative sizes, boundary energies and mobility of the grains [Humphery 1977].

Figure 1.20 gives conditions for distributions of grain growth, mobility ratio, and surface energy ratio. Microstructural instability can occur in the material when Q>G but it will be minimum if X=2G=2Q and Q=G. Abnormal grain growth is easier in thin sheets rather than bulk material because surface tension and grain boundary tension may exert pinning effect on boundary [Humphrey et al. 1995]. Where mobility ratio $Q = M/\bar{M}$, size ratio $X = R/\bar{R}$ and energy ratio $G = \gamma/\bar{\gamma}$. Hence, M, X and γ

are mobility of boundary, radius and grain boundary energy of particular grain but $\overline{M}$, $\overline{R}$ and $\overline{\gamma}$ are mean values for all the grains respectively.

1.9 Applications of UFG Materials

A generation of new and unusual properties has been demonstrated for wide range of UFG metals and alloys including enhanced functional (electric, magnetic and corrosion properties etc), medical properties and many other [Estrin, Vinogradov, et al. 2013, Valiev Langdon, Terence et al. 2014, Valiev, Sabirov, Zhilyaev, Langdon et al. 2012, Langdon 2013]. One can find nano Ti alloys for bimodal applications, nano structured Cu and Al alloys for prospective electroconductors, nono structured Mg alloys for hydrogen storage, micro devices from bulk nano structured materials and nano magnets for high speed electric machines. Nano structured Ti has been established under the trade marks: Samurai metals TM (Metallium nano crystalline rods), NanoMet Ltd. (NanoMet-rods), Nanoimplanet TM (Timplant-dental implants) and Biotanium TM (Basic Dental Inc-dental implants). Applications of SPD materials include aerospace, automotive, aircraft, medical, sport, oil and gas and infracture [Gupta 2014]. Nano SPD aluminium alloys have high potential and high strength for application in aerospace, power and automotive industries [Muley et al. 2015]. Joo et al. [Joo et al. 2010] have used high pressure torsion processing to produce homogeneous nano structures with high angle grain boundaries in carbon nanotube/Al composites due to its ability to impose extremely high strain and hydrostatic pressure. Aluminum matrix hybrid composite reinforced with tungsten oxide particles and Aluminium borate whiskers ($Al_{18}B_4A_{33}$) possess superior stiffness and strength. $Al_{18}B_4A_{33}$ reinforced Al matrix composite are used in automobile shaft and brake rotors. Strength of this composite increase from 47.9 MPa to 287 MPa with 1.6% total elongation with highly dense and homogeneous distribution of Tungsten Oxide in the

matrix [Feng et al. 2008]. Manufacturing of some components is promising like aircraft fuselage (Stringers, skin plates), sections of various geometries and sheets for assemblies operating in corrosive environment at cryogenic temperature [Tooren et al. 2007]. UFA Russia has models of hollow blades of grain size below 0.2 μm by diffusion bonding and superplastic forming using UFG Ti-6Al-4V sheets. By using this for superplastic forming process, temperature got reduced from 900 to 700°C, which increased technical feasibility and economics of process [Kaibyshev et al. 2006]. The ECAE process is utilized to manufacture the high strength bolt with less weight using the UFG AA6061. These bolts were prepared by the route A after four passes and tensile strength improved to 302 MPa compared to 168 MPa of the conventional AA2024 Al alloy [Choi et al. 2011]. UFG Al 5083 plate containing bimodal grain size distribution, 600–700 MPa yield strength and 11% elongation and 33% improvement in the ballistic performance was obtained by cryogenic ball milling, consolidation by hot isostatic pressing, forging and finally rolling [Newbery et al. 2006]. These UFG Al plate is expected to be used for lighter armor plates and armor penetrators for the reduction of fuel consumption, higher speed, better manoeuvrability, longer operation range and air-transport of vehicles to remote locations [Azushima et al. 2008]. Substantially improved fatigue lifetimes [Estrin et al. 2013] and increased damage tolerances [Kumara et al. 2003] will pave the way for industrial applications. A stable SUS316L austenitic stainless steel is deformed by ECAP processing at 150°C, following route Bc for excellent fatigue performance and impressive thermal stability. Microstructure exhibited nano scale grain structure with 100 nm grain boundaries and intersecting twin lamellae [Ueno et al. 2011].

1.10 Objectives of Thesis

The objectives of the present investigation are to produce bulk ultrafine-grained (UFG) interstitial-free steel of high strength and high ductility, using a severe plastic deformation method of equal-channel angular pressing (ECAP) followed by coldrolling or cryorolling and thermal treatments. Interstitial-free steel being one of the major materials for automotive structures is selected for their improvement in mechanical properties. Till now IF steel has been deformed by ECAP process upto an equivalent strain of 9.2. Therefore, the aim of present work is to focus on the microstructural development of IF steel by ECAP at low to large equivalent strain beyond 9.2 and their impact on mechanical properties, specially, on tensile strength, ductility, hardness and fracture behaviour. So far texture analysis of IF steels upto equivalent strain 9.2 has been reported. Properties of material are strongly dependent on microstructure and anisotropy. Controlling of texture and microstructure are important in SPD processes under large strain and strain path. Therefore, the other aim of present investigation is to focus on texture development at large strain level and their correlations with microstructural changes. The other objective of present investigation also involves changing mode of deformation from ECAP to coldrolling/cryorolling to further increase dislocation density, refine the microstructure and enhance strength. The properties required for structural applications are ultra high strength and high toughness (or ductility). Reduction in grain size of alloys to ultrafine range by ECAP enhances yield strength to ultra high range but unfortunately ductility is much lower than that of their coarse grained counterpart though it is much higher than that of nano size range. The lower ductility in UFG materials is due to lack of dislocation activities. To optimize the strength and the ductility, the microstructure will be modified to get bimodal grain size of

ultrafine-grains to maintain ultra high strength and micron sized grains to accommodate plastic deformation. Such microstructure will be optimised by controlling the ECAP parameters along with post ECAP processing followed by thermal treatments. Further post annealing conditions should be standardized to study the thermal stability of ultrafine-grained IF steel. Finally processing conditions, microstructure and mechanical properties will be correlated.